Optics Letters

Optical transfer function engineering for a tunable 3D structured illumination microscope

Hasti Shabani,[1] Ana Doblas,[1] Genaro Saavedra,[2] and Chrysanthe Preza[1,*]

[1]Computational Imaging Research Laboratory, Department of Electrical and Computer Engineering, University of Memphis, Memphis, Tennessee 38152, USA
[2]3D Imaging and Display Laboratory, Department of Optics, University of Valencia, Burjassot, E-46199, Spain
*Corresponding author: cpreza@memphis.edu

Received 21 December 2018; accepted 13 February 2019; posted 20 February 2019 (Doc. ID 356018); published 19 March 2019

Two important features of three-dimensional structured illumination microscopy (3D-SIM) are its optical sectioning (OS) and super-resolution (SR) capabilities. Previous works on 3D-SIM systems show that these features are coupled. We demonstrate that a 3D-SIM system using a Fresnel biprism illuminated by multiple linear incoherent sources provides a structured illumination pattern whose lateral and axial modulation frequencies can be tuned separately. Therefore, the compact support of the synthetic optical transfer function (OTF) can be engineered to achieve the highest OS and SR capabilities for a particular imaging application. Theoretical performance of our engineered system based on the OTF support is compared to that achieved by other well-known SIM systems.

https://doi.org/10.1364/OL.44.001560

Three-dimensional structured illumination microscopy (3D-SIM), in which the structured illumination (SI) pattern varies laterally and axially, has become one of the most effective optical imaging modalities used in biological investigations because of its optical sectioning (OS) and super-resolution (SR) capabilities. The SI pattern in a 3D-SIM system has been traditionally implemented by interfering three coherent waves (3W-SIM) [1] and recently using a tunable-frequency incoherent illumination based on a Fresnel biprism (tunable-SIM) [2]. It has been demonstrated experimentally that 3W-SIM can double both the lateral and axial resolution limits while providing OS capability [1]. As expected, the choice of the lateral modulation frequency of the SI pattern in 3W-SIM determines the final performance (i.e., achieved lateral and axial SR and OS capabilities) because in 3W-SIM, the axial and lateral modulation frequencies are coupled. Therefore, the system's performance would be compromised if the highest lateral modulation frequency cannot be used (e.g., when an optically thick sample is imaged, the contrast of the SI pattern can be severely reduced, necessitating the use of a lower modulation frequency [3,4]). We have recently shown that the 3W-SIM and the tunable-SIM systems have comparable performance at the highest possible modulation frequency by noisy simulation of a particular numerical object used in this study [2]. However, the lateral and axial modulation frequencies of the tunable-frequency 3D pattern can be controlled separately by system parameters, which is not the case in the 3W-SIM system. This unique property allows us to engineer the synthetic optical transfer function (OTF) of the tunable-SIM system for a desired imaging application.

In this Letter, we investigate the performance of our novel tunable-SIM system [2] based on the achieved extension of the compact support of its synthetic OTF, which is controlled by system parameters. These parameters can be chosen to design the pattern and thereby engineer the synthetic OTF. To our knowledge, this is the first 3D-SIM setup that enables independent control of the achieved OS and SR capabilities. The analysis of the system's performance is evaluated through its synthetic OTF. Based on the approach previously used to derive the 2D-SIM synthetic OTF [5], we formulate the synthetic OTF of a 3D-SIM system, $H_{\mathrm{SIM}}(\mathbf{u}, w)$, when the 3D SI pattern is separable into a transverse and axial function (as it is the case for the 3W-SIM and tunable-SIM systems), as

$$H_{\mathrm{SIM}}(\mathbf{u}, w) = H(\mathbf{u}, w) \otimes_3 I(\mathbf{u}, w), \tag{1}$$

where $\mathbf{u} = (u, v)$ and w are, respectively, the lateral and axial spatial frequency coordinates, $H(\mathbf{u}, w)$ is the conventional OTF, and $I(\mathbf{u}, w)$ is the Fourier transform (FT) of the 3D SI pattern. In our tunable-SIM system, axially localized high-contrast sinusoidal patterns are generated by incoherent overlapping of axially extended interference patterns produced by a set of equidistant parallel incoherent linear sources (slits) and a Fresnel biprism [2]. This incoherent superposition produces a 3D SI pattern that is axially periodic. The 3D SI pattern in the sample volume is given by [2]

$$i(\mathbf{x}, z) \approx 1 + V(z) \cos(2\pi u_m x + \varphi), \tag{2}$$

where $\mathbf{x} = (x, y)$ and z denote the lateral and axial coordinates, respectively; φ is the phase of the illumination pattern shifted by laterally translating the Fresnel biprism [2]; and

$$\mathcal{V}(z) = \frac{\sin(2\pi N w_m z)}{N \sin(2\pi w_m z)}, \tag{3}$$

defined as the visibility function [2], depends on the number of slits N, and on the lateral and axial modulation frequencies, $u_m = [2\eta(n_F - 1)\tan\delta]/[\lambda f_{L1} M_{\mathrm{ill}}]$, and $w_m = [x_0 u_m]/[2 f_{L1} M_{\mathrm{ill}}]$, respectively, determined by the system (Fig. 1 in Ref. [2]):

excitation wavelength (λ), biprism position (η), focal length of the first converging lens (f_{L1}), lateral magnification of the illumination system (M_{ill}), biprism refingence angle (δ) and refractive index (n_F), and the distance between two neighboring slits (x_0). Although Eq. (2) shows the lateral modulation only in one direction, modulation in other lateral directions can be achieved by rotating the 3D SI pattern laterally [2].

As mentioned earlier, the lateral and axial modulation frequencies of the 3D SI pattern can be controlled separately. The lateral modulation frequency (u_m) can be tuned, up to the effective cutoff frequency of the system ($u_{c\text{-eff}} = 0.8u_c$, in which u_c is the cutoff frequency of the WFM), by axially changing the position of the Fresnel biprism (η) with regard to the slits' plane. Although the axial modulation frequency (w_m) depends on u_m, it can be tuned independently by selecting x_0 in the design of the slits element while keeping u_m constant. The space and frequency representations of our tunable 3D pattern [Eq. (2)] are shown in Figs. 1(a) and 1(c), respectively. The blue profile plotted in Fig. 1(a) represents the absolute value of the visibility function [Eq. (3)]. We observe that the fringes' visibility is a periodic function that takes its maximum value [$V(z) = 1$] at a discrete set of axial planes, referred to as the resonant planes. The separation between resonant planes, $T = 1/w_m$, is inversely proportional to η and x_0 but independent of N [Fig. 1(a)]. On the other hand, the axial extent of the fringes [$\Delta_z = 2/(Nw_m)$], defined by the region around the resonant planes in which $V(z) = 0$, decreases with increasing N, x_0, and η. Note that the FT of Eq. (3), $V(w)$, is given by

$$V(w) = \frac{1}{N}\sum_{n=0}^{N-1}\delta[w - (2n - N + 1)w_m]. \tag{4}$$

Inserting the FT of Eq. (2) in Eq. (1), the synthetic OTF of the tunable-SIM system can be expressed by

$$H_{\mathrm{SIM}}(\mathbf{u}, w) = H(\mathbf{u}, w) + \sum_{n=0}^{N-1}\frac{H[u \pm u_m, v, w - (2n - N + 1)w_m]}{2N}, \tag{5}$$

which is the sum of the conventional wide-field fluorescence microscope (WFM) OTF and two new components, each composed by the sum of N axially shifted replicas of the conventional OTF separated by $2w_m$, that are shifted laterally by $\pm u_m$ [Fig. 1(d)]. Note that the number and the location of the replicas in the synthetic OTF [Fig. 1(c)] change with the number of slits (N), and the distance between two neighboring slits (x_0), respectively. However, there is still one single lateral modulation frequency (u_m) for all the replicas. Therefore, only three images per orientation of the SI pattern are needed to reconstruct SR images with the tunable-SIM system, independent of the number of slits (N) or other system parameters (x_0 and η). Taking advantage of the independent tuning of u_m and w_m, it is possible to engineer the synthetic OTF's compact support by selecting parameters (N, x_0, η) for a specific SI design.

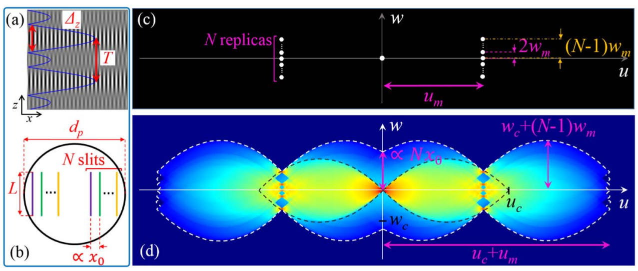

Fig. 1. Relation of the SI design and synthetic OTF of the tunable-SIM system. (a) *xz* section of 3D SI pattern and the $|\mathcal{V}(z)|$ (blue curve) of Eq. (3). (b) Schematic of the slit-element image at the back focal plane of the objective lens. (c) *uw* section of the 3D pattern's FT. (d) *uw* section of the synthetic MTF for $u_m = u_{c\text{-eff}} = 0.8u_c$. OTF compact support for WFM and tunable-SIM shown by black and white dashed lines, respectively.

Because it is desired to operate at the highest lateral SR performance, the η-parameter should be fixed to provide SI fringes with the highest lateral modulation frequency $u_m = u_{c\text{-eff}} = 0.8u_c$ (this is also the highest frequency usable for 3W-SIM as demonstrated in [6]). This is because at this frequency, the fringes' contrast is attenuated by a factor of 0.1 due to the incoherent detection OTF for fluorescence imaging [7]. Figure 1(d) shows the *uw*-section image of the synthetic modulation transfer function (MTF), absolute modulus of the OTF, of our tunable-SIM system, for the general case of N slits (separated by a distance x_0). From this figure, one realizes that both lateral and axial OTF compact support (white dashed line) have been extended compared to the compact support of the conventional OTF (black dashed line). Note that the lateral and axial resolution limits [pink arrows in Fig. 1(d)] have been increased by a factor of $1 + (u_m/u_c)$ and $1 + [(N - 1)(w_m/w_c)]$, respectively, where $u_c = 2\,\mathrm{NA}/\lambda$ and $w_c = \mathrm{NA}^2/(2n\lambda)$ are the lateral and axial cutoff frequencies of the WFM system, respectively. Note that NA is the lens' numerical aperture, and n is the refractive index of the lens' immersion medium. In addition to the lateral and axial extension of the OTF, Fig. 1(d) shows that the upper portion of the missing cone of frequencies in the conventional OTF is filled by $N/2$ axially shifted WFM OTF replicas, with axial separation between two neighboring replicas equal to $2w_m$. Therefore, the amount of the missing cone that has been filled is quantified by Nw_m. This means that (1) the higher the number of slits and/or (2) the larger the separation between two neighboring OTF replicas (i.e., larger w_m), the better the OS capability of the system. Because w_m is proportional to x_0, the product Nx_0 can be used as a metric in synthetic SIM-OTF engineering. It is worth realizing that this metric, Nx_0, is related to Δ_z in the reciprocal space; a smaller Δ_z allows greater discrimination of out-of-focus information.

Although increasing the number of slits (N) provides higher axial SR and better OS capability there is a limit in a realistic experiment. There is an upper limit for the N value determined by the pupil's diameter (d_p) of the objective lens used, given by

$$N_{\max} = 1 + \left(1 - \frac{u_m}{u_c}\right)\frac{f_{L1}\sqrt{d_p^2 - L^2}}{f_{L2}x_0}, \tag{6}$$

where L is the slits' length at the pupil plane and needs to fit entirely within the aperture stop of the objective lens [Fig. 1(b)] to avoid clipping of the slits' image and, consequently, fringes with reduced contrast [2]. For example, the maximum number of slits for a $20\times/0.5$ NA dry objective lens is $N_{\max} = 9$, assuming $x_0 = 100$ μm, $u_m = 0.8u_c$, and a lateral magnification between the slits and pupil planes of $M = -f_{L2}/f_{L1} = -2.5$.

Figures 2(a) and 2(b) show the synthetic MTF for two different numbers of slits, where the image intensities are normalized and mapped to the same color scale (a similar intensity normalization is used in Figs. 3 and 4). From these panels, one realizes that the lateral cutoff frequency of the synthetic OTF is invariant with the N value and always remains at the maximum value of $2u_{c\text{-eff}}$. On the other hand, the axial cutoff frequency increases with the number of slits. Particularly, the axial resolution increases by a factor of 1.5× when the number of slits is increased from $N = 3$ [Fig. 2(a)] to 9 [Fig. 2(b)].

The OS capability is investigated through the integrated intensity function [Fig. 2(d)], which forms a Fourier pair [5] with the axial OTF, $H(\mathbf{u} = \mathbf{0}, w)$, in any imaging system. Because the first term in the right-hand side of Eq. (5) is the WFM OTF and it lacks OS capability, in what follows, we compute the integrated intensity profiles by neglecting this term. In addition, the axial distance is normalized by $4k \sin^2[\sin^{-1}(\mathrm{NA}/n)/2]$, where $k = 2\pi/\lambda_n$ is the wave vector in the lens' immersion medium of refractive index n. As expected, the system using nine slits provides better OS capability (narrower integrated intensity) compared to the systems with $N = 3$. This is quantified by measuring the half width at half-maximum (HWHM) of the integrated intensity profiles [Fig. 2(d)], found to be equal to 6.84 and 3.95 for $N = 3$ and $N = 9$, respectively. The theoretical OS performance of the tunable-SIM system with $N = 9$ slits is validated experimentally and numerically. Figure 2(d) shows the integrated intensity of the experimental (gray dashed line) and numerical (orange dashed line) demodulated SIM images from an axially thin fluorescent layer [2]. The OS performance can be further improved by applying deconvolution to the demodulated image [Fig. 2(d), gray and orange solid lines].

Although we have demonstrated that both the axial SR and the OS capability improve by increasing the number of slits, it is interesting to point out that similar OS performance can be achieved with a lower number of slits by increasing x_0 so that the product Nx_0 is kept constant. Figures 2(b) and 2(c) show the synthetic OTF's compact support and the integrated intensity for two different cases in which $Nx_0 = 900$ μm. Note that although Nx_0 is fixed, the axial modulation frequency w_m is different for each case providing a different axial SR. Although the difference in the HWHM values of the integrated intensity profiles for these two cases is negligible (<4%), some difference in the secondary lobes of the integrated intensity curves is evident [Fig. 2(d)], and it is quantified by the normalized second-order moment (σ_2), which classically it has been used to assess the global width of a function [8]. Considering both the HWHM and σ_2 metrics, then the system with the best OS performance is the one with a slit element of $N = 9$ and $x_0 = 100$ μm [Fig. 2(d)]. Another difference is the attenuation of the frequencies located at the border of the synthetic OTF [regions indicated by red arrows in Figs. 2(b) and 2(c)], which is less for the design with $N = 3$ and $x_0 = 300$ μm. This attenuation is related to the $1/N$ factor in Eq. (5), and it potentially renders the system more sensitive to noise at high frequencies for higher N values. Thus, there is a trade-off between the optimal slit-element design (N and x_0) and the system's robustness to noise.

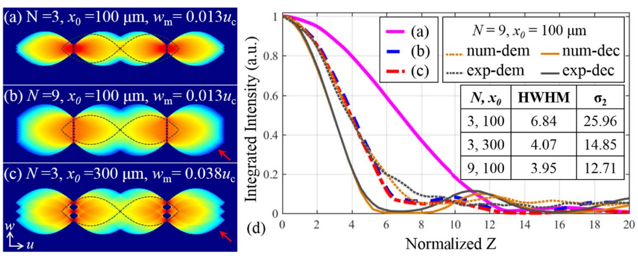

N, x_0	HWHM	σ_2
3, 100	6.84	25.96
3, 300	4.07	14.85
9, 100	3.95	12.71

Fig. 2. Impact of slits' parameters (N and x_0) on the synthetic OTF's compact support and OS capability of the tunable-SIM system. (a)–(c) uw section of the synthetic MTF for different designs. (d) Integrated intensity profiles of (a)–(c), experimental (exp) and numerical (num) results. Legends, "dem" and "dec" stand for demodulated and deconvolved, respectively. For this study we used $u_m = u_{c\text{-eff}} = 0.8u_c$.

Theoretical predictions of the SR and OS capabilities of the tunable-SIM system are compared with the ones achieved by other well-established systems: the 3W-SIM [1], the incoherent grid-projection OS-SIM [9], and the confocal microscope [10]. For the case of the OS-SIM system, we have considered the highest theoretical lateral modulation frequency $u_m = 0.5u_c$ that can be used [9]. Regarding the confocal scanning system, we assumed an ideal pinhole and that the Stokes shift is 0.8 [5]. To provide an extensive comparison between the 3W-SIM and the tunable-SIM systems, we considered two different lateral modulation frequencies ($u_m = 0.5u_c$ and $u_m = 0.8u_c$), because when imaging optically thick samples, there is a need to reduce the lateral modulation frequency to modulate the sample's information [3,4]. In 3W-SIM systems, this reduction has been alleviated by either line scanning the sample laterally [11] or by combining a Bessel beam to the SIM system [12].

The uw-section images of the synthetic OTF for the tunable-SIM and 3W-SIM systems are shown in Figs. 3(a)–3(e). From these images, one can realize that both systems provide the same lateral SR improvement for the same lateral modulation frequency of the SI pattern. However, the axial SR and OS capabilities are different depending on the lateral modulation frequency. Note that for each chosen slit element design of the tunable-SIM system, we determine the maximum distance between two neighboring slits (x_0) for a specific N and u_m using Eq. (6). For $u_m = 0.8u_c$, the synthetic OTFs of both 3D-SIM systems [Figs. 3(a) and 3(b)] have the same axial extension, and, thereby, both systems provide the same SR improvement along the lateral and axial directions. Notwithstanding, the OS capability is slightly different as one realized from the integrated intensity curves [Fig. 3(f)]. Depending on the metric used, the HWHM and the normalized second-order moment

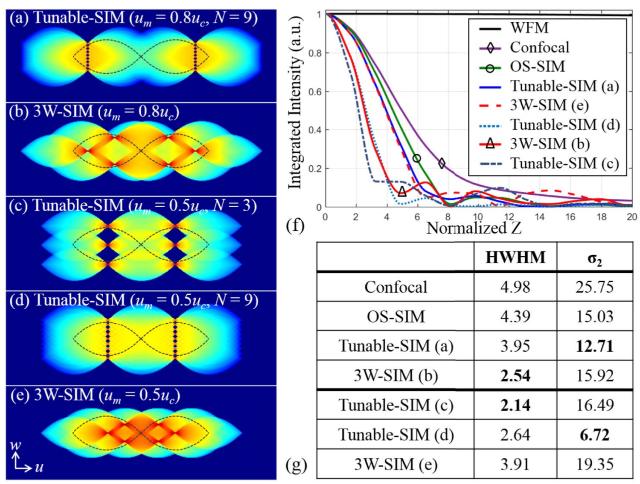

	HWHM	σ_2
Confocal	4.98	25.75
OS-SIM	4.39	15.03
Tunable-SIM (a)	3.95	**12.71**
3W-SIM (b)	**2.54**	15.92
Tunable-SIM (c)	**2.14**	16.49
Tunable-SIM (d)	2.64	**6.72**
3W-SIM (e)	3.91	19.35

Fig. 3. Comparison of different systems' performance. (a–e) uw section of the synthetic MTF for tunable-SIM and 3W-SIM systems at different designs. (f) Integrated intensity profiles obtained from the MTF of the systems (a)–(e), OS-SIM ($u_m = 0.5u_c$), confocal microscope, and WFM. (g) HWHM and σ_2 values computed from integrated intensity curve.

(σ_2) of the integrated intensity, one could conclude that either the 3W-SIM system or our 3D-SIM system provides the highest OS capability. Nonetheless, overall, the OS capability of both systems operating at $u_m = 0.8u_c$ is quite comparable and as expected higher than the one provided by the confocal and incoherent grid-projection SIM [Fig. 3(f)]. However, we believe that our proposed system could have a significant impact when low and medium lateral modulation frequencies are needed. Figure 3 shows that the tunable-SIM system (with either SI design) operating at $u_m = 0.5u_c$ presents the highest axial SR (axial OTF extension of $w_c + 0.144u_c$) and OS capabilities among all investigated systems. Therefore, designing the slit element, we can engineer the frequency response of our system to always operate at the highest performance for a given imaging application.

Finally, we study how noise affects both 3D-SIM systems, as their synthetic OTFs have a different strength. In fluorescent imaging, shot noise is the dominant noise source, and it is considered to be Poisson distributed [13]. For this study, the image of a subresolved bead, which represents the WFM point spread function (PSF), was scaled to mimic a specific photon count, and it was used to generate Poisson noise. Since this model for the noise is spatially variant, the global noise level, as quantified by the signal-to-noise ratio (SNR), is computed by taking the average over the whole PSF. According to Poisson statistics, this value corresponds to the mean of the squared root of the intensity at each pixel in the 3D image. A noisy WFM MTF was generated by taking the absolute value of the FT of the noisy WFM PSF. The noisy synthetic SIM MTF was then generated from the noisy WFM MTF using Eq. (5) for the tunable-SIM case, while for the 3W-SIM case Eq. (1), with the corresponding SI pattern was used instead. Figures 4(a)–4(d) show the noisy synthetic MTFs (the average of a 100-realizations ensemble) of two designs of the tunable-SIM and the 3W-SIM systems for two modulation frequencies and at two different SNR levels. The noise effect is quantified by determining the effective lateral and axial cutoff frequencies as the limiting frequencies at which the noiseless synthetic MTF value falls below a threshold. The threshold value was set equal to the background mean value of the noisy synthetic MTF beyond the noiseless axial and lateral cutoff frequencies. As shown in Figs. 4(e) and 4(f), although both systems perform equally well for a high SNR (>20 dB for $u_m = 0.8u_c$ and >15 dB for $u_m = 0.5u_c$), their performances are different at low SNR values. For SNR = 10 dB and $u_m = 0.8u_c$, there is a 12% and 20% reduction in the effective axial cutoff frequency in the 3W-SIM and tunable-SIM, respectively [Fig. 4(f)], while the reduction in the effective lateral cutoff frequency is less in the tunable-SIM [e.g., 13% and 17% reduction for tunable-SIM and 3W-SIM, respectively, in Fig. 4(e)]. This is because the different arrangements of the WFM OTF replicas results in a different synthetic OTF value in each system. On the other hand, for $u_m = 0.5u_c$, although the 3W-SIM system performs slightly better laterally for SNR < 10 dB, (e.g., 36% and 45% reduction in the effective lateral frequency for 3W-SIM and tunable-SIM, respectively, when SNR = 5 dB), the tunable-SIM system outperforms 3W-SIM at all SNR levels with axial resolution improvement by a factor of 2.2× compared to the 1.6× improvement achieved by the 3W-SIM system.

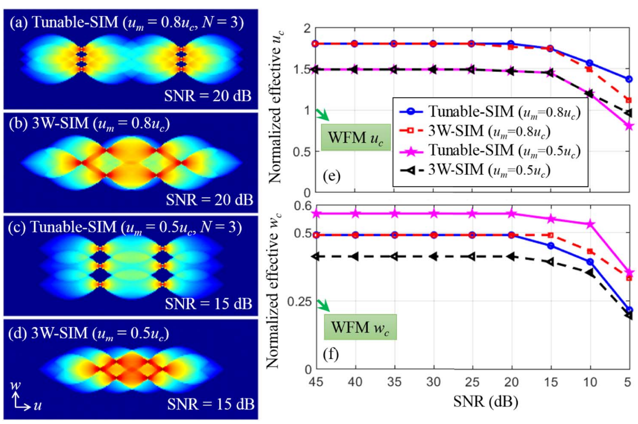

Fig. 4. Performance of two 3D-SIM systems under noisy conditions. *uw* section of the synthetic MTF for tunable-SIM and 3W-SIM systems for (a–b) SNR = 20 dB and (c–d) SNR = 15 dB. Effective (e) lateral and (f) axial cutoff frequencies for different SNR levels.

In summary, we presented a unique tunable SI system that can be engineered for use in a 3D-SIM system that provides 40% reduction in data acquisition compared to the 3W-SIM system [2]. Here we investigated different SI designs in terms of the OS and SR capabilities of the tunable-SIM system and showed that the lateral and axial modulation frequencies of this SI pattern can be controlled separately by system parameters. This unique property allows us to engineer the synthetic OTF of the system for a desired imaging application by designing the slit element, so that our 3D-SIM system operates at the highest axial SR and OS capabilities even though the lateral SR must be reduced. We believe that our system will have a high impact in those biological imaging applications where the highest lateral modulation frequency cannot be used due to a reduction in the SI pattern's contrast.

Funding. National Science Foundation (NSF) (DBI award 1353904, PI: CP); Ministerio de Economía y Competitividad (MINECO) (DPI2015-66458-C2-1-R); Generalitat Valenciana (PROMETEOII/2014/072).

REFERENCES

1. M. G. L. Gustafsson, L. Shao, P. M. Carlton, C. J. R. Wang, I. N. Golubovskaya, W. Z. Cande, D. A. Agard, and J. W. Sedat, Biophys. J. **94**, 4957 (2008).
2. A. Doblas, H. Shabani, G. Saavedra, and C. Preza, Opt. Express **26**, 30476 (2018).
3. M. F. Langgorst, J. Schaffer, and B. Goetze, Biotechnol. J. **4**, 858 (2009).
4. D. Débarre, E. J. Botcherby, M. J. Booth, and T. Wilson, Opt. Express **16**, 9290 (2008).
5. M. Martínez-Corral and G. Saavedra, in *The Resolution Challenge in 3D Optical Microscopy* (Elsevier, 2009), Vol. **53**, pp. 1–67.
6. C. Karras, M. Smedh, R. Förster, H. Deschout, J. Fernandez-Rodrigue, and R. Heintzmann, Opt. Commun. **436**, 69 (2019).
7. J. W. Goodman, *Introduction to Fourier Optics* (McGraw-Hill, 1966).
8. I. Escobar, E. Sanchez-Ortiga, G. Saavedra, and M. Martinez-Corral, in *Optical Fluorescence Microscopy: From the Spectral to the Nano Dimension* (Springer, 2011), pp. 85–99.
9. M. A. A. Neil, R. Juskaitis, and T. Wilson, Opt. Lett. **22**, 1905 (1997).
10. L. H. Schaefer and D. Schuster, "Method and device for reconstructing images," U.S. patent 8,041,142 (October18, 2011).
11. O. Mandula, M. Kielhorn, K. Wicker, G. Krampert, I. Kleppe, and R. Heintzmann, Opt. Express **20**, 24167 (2012).
12. N. Hagen, L. Gao, and T. S. Tkaczyk, Opt. Express **20**, 5343 (2012).
13. D. L. Snyder, R. L. White, and A. M. Hammoud, J. Opt. Soc. Am. A **10**, 1014 (1993).